



**Pacific
Northwest**
NATIONAL LABORATORY

PNNL-35705

Optimal Control for Fast Frequency Response and Black-Start using Embedded Storages with Grid-Forming Control

Quan Nguyen
Xue Lyu
Meng Zhao
Jessica Kerby
Laurentiu D Marinovici
Diane Baldwin

U.S. DEPARTMENT OF
ENERGY

Prepared for the U.S. Department of Energy
Under contract DE-AC05-76RL01830

DISCLAIMER

This report was prepared as an account of work sponsored by an agency of the United States Government. Neither the United States Government nor any agency thereof, nor Battelle Memorial Institute, nor any of their employees, makes **any warranty, express or implied, or assumes any legal liability or responsibility for the accuracy, completeness, or usefulness of any information, apparatus, product, or process disclosed, or represents that its use would not infringe privately owned rights.** Reference herein to any specific commercial product, process, or service by trade name, trademark, manufacturer, or otherwise does not necessarily constitute or imply its endorsement, recommendation, or favoring by the United States Government or any agency thereof, or Battelle Memorial Institute. The views and opinions of authors expressed herein do not necessarily state or reflect those of the United States Government or any agency thereof.

PACIFIC NORTHWEST NATIONAL LABORATORY
operated by
BATTELLE
for the
UNITED STATES DEPARTMENT OF ENERGY
under Contract DE-AC05-76RL01830

Printed in the United States of America

Available to DOE and DOE contractors from
the Office of Scientific and Technical Information,
P.O. Box 62, Oak Ridge, TN 37831-0062

www.osti.gov

ph: (865) 576-8401

fox: (865) 576-5728

email: reports@osti.gov

Available to the public from the National Technical Information Service
5301 Shawnee Rd., Alexandria, VA 22312

ph: (800) 553-NTIS (6847)

or (703) 605-6000

email: info@ntis.gov

Online ordering: <http://www.ntis.gov>

Optimal Control for Fast Frequency Response and Black-Start using Embedded Storages with Grid-Forming Control

Quan Nguyen
Xue Lyu
Meng Zhao
Jessica Kerby
Laurentiu D Marinovici
Diane Baldwin

Prepared for
the U.S. Department of Energy
Under Contract DE-AC05-76RL01830

Pacific Northwest National Laboratory Richland, Washington 99352

Acknowledgement

This material is based upon work supported by the US Department of Energy's Office of Renewable Energy and Energy Efficiency under the Office of Strategic Programs under award number 39650.

Contents

Abstract	vi
1.0 Optimal Control of Embedded Storages with Grid-Forming Control for Fast Frequency Response	1
1.1 Introduction	1
1.2 Problem Formulation	1
1.3 Case Studies	3
1.4 Conclusion	4
2.0 Optimal Scheduling of Mobile Embedded Storages with Grid-Forming Control for Black-Start	7
2.1 Background & Inspiration	7
2.2 New Problem Formulation	7
2.2.1 Assumptions	7
2.2.2 Modeling of mobile embedded storages	7
2.2.3 Variables of the system	8
2.2.4 Objective function	8
2.2.5 Constraints	8
2.3 Simulation Results	9

Abstract

The grid-forming inverter is regarded as the solution for integrating high levels of renewable resources into future power systems. Ensuring the stable operation of grids necessitates that grid-forming inverters offer fast frequency response. This report introduces an optimal control method that coordinates the embedded storage within the grid-forming control model with conventional synchronous generators. The optimized active power reference for the embedded storage is generated using receding horizon optimization control, aiming to keep the center of inertia frequency within acceptable limits. The effectiveness of the proposed control is verified through testing in the IEEE 39-bus system. In addition, with grid-forming capability, we will also investigate the application of using mobile embedded storages as black-start units to provide cranking power to energize non-blackstart generators in a black-start process.

1.0 Optimal Control of Embedded Storages with Grid-Forming Control for Fast Frequency Response

1.1 Introduction

With the rising penetration of renewable generation, numerous new challenges arise. Unlike conventional synchronous generators (SGs), distributed units connect to the grid via power inverters, which offer fast response and decouple the kinetic energy stored in rotational mass from the grid. Consequently, they cannot provide inertial response. Additionally, they lack primary reserve as they typically operate in maximum power tracking (MPPT) mode. These characteristics can have a negative impact on system frequency dynamics when disturbances occur. Energy storage devices could provide a solution to mitigate this problem, as they can offer fast frequency response.

Grid-forming (GFM) control has gained increasing attention due to its ability to establish a stable voltage without relying on other resources. Among existing approaches, droop control and virtual synchronous machine (VSM) are the two main methods employed for GFM control. Droop control utilizes classical $P - \omega$ and $Q - V$ droop to regulate the inverters' active and reactive power output [1, 2]. VSM control, on the other hand, employs the swing equation of SGs to mitigate transient system dynamics [3].

Explicit models of grid-following (GFL) and GFM devices are developed in [4] for inertia emulation and fast frequency response. In this work, feedback control loops are designed to provide virtual inertia and damping. Additionally, in [5], an optimal feedback adaptive virtual inertia controller based on linear-quadratic regulator (LQR) is designed. This controller adjusts the emulated inertia and damping constants according to the frequency disturbance in the system, while maintaining a balance between critical frequency limits and the required control effort. A rule-based approach is presented in [6] for GFM power converters, in which the virtual inertia and damping are adjusted based on the normal operation mode or faulted operation mode following a disturbance.

The approach to controlling the storage system in GFM mode in response to disturbances remains an open question. In this study, we employ VSM control to enable the storage to emulate SGs behavior. In addition to providing the inertial response, in this work, we generate an additional optimal control signal for the storage, taking into account the dynamics of the system frequency. Our control strategy relies on receding horizon optimization, wherein we incorporate frequency deviation and the rate of change of frequency (RoCoF) as constraints. This study encompasses two control objectives: minimizing the control effort of the storage system and enhancing frequency behavior. The proposed method is evaluated using an IEEE 39-bus system.

1.2 Problem Formulation

For synchronous generators, a fourth-order model is utilized in this study,

$$\frac{d}{dt}\theta_{g,i} = \omega_{g,i} \quad (1)$$

$$2H_{g,i}\frac{d}{dt}\omega_{g,i} = P_{m,i} - P_{eg,i} - D_{g,i}(\omega_{g,i} - \omega_{\text{ref}}) \quad (2)$$

$$T_{t,i}\frac{d}{dt}P_{m,i} = P_{g,i} - P_{m,i} \quad (3)$$

$$T_{g,i}\frac{d}{dt}P_{g,i} = -P_{g,i} - \frac{(\omega_{g,i} - \omega_{\text{ref}})}{R_i} \quad (4)$$

$$P_{eg,i} = \sum_{j \in n_n} B_{ij}(\theta_{g,i} - \theta_j), \quad (5)$$

where $\delta_{g,i}, \omega_{g,i}$ represent the phase angle and frequency, $H_{g,i}, D_{g,i}, R_i$ represent inertia constant, damping coefficient, and droop coefficient, $P_{m,i}, P_{g,i}$ represent mechanical power and governor output, and $T_{t,i}, T_{g,i}$ are turbine and governor time constants of the i -th generator. $P_{eg,i}$ represents the electric power, which is calculated via DC power flow in (5), where δ_j is the phase angle of bus j .

For the VSM controlled grid-forming embedded storage, its mathematical model can be expressed as,

$$\frac{d}{dt}\theta_{es,s} = \omega_{es,s} \quad (6)$$

$$2H_{es,s}\frac{d}{dt}\omega_{es,s} = P_{ref,s} - P_{f,s} - (D_{es,s} + \frac{1}{m_{p,s}})(\omega_{es,s} - \omega_{ref}) \quad (7)$$

$$T_{f,s}\frac{d}{dt}P_{f,s} = -P_{f,s} + P_{ees,s} \quad (8)$$

$$P_{ees,n} = \sum_{j \in n_n} B_{sj}(\theta_{es,s} - \theta_j), \quad (9)$$

where $\theta_{es,s}, \omega_{es,s}$ represent the phase angle, frequency, $H_{es,s}, D_{es,s}, m_{p,s}$ represent the inertia constant, damping constant, droop coefficient, $P_{ref,s}, P_{f,s}, P_{ees,s}$ represent the active power reference, the measured active power through low-pass filter, the electric power of the s -th storage. $T_{f,s}$ represents the time constant of the low pass filter.

Utilizing the mathematical models of the conventional synchronous generator and the embedded storage mentioned above, this study employs receding horizon control to optimize storage operation. Employing zero-hold discretization, the discretized dynamics of the synchronous generator and the storage can be expressed as follows:

$$\Delta x(k+1) = A_d \Delta x(k) + B_d \Delta u(k) + F_d \Delta w(k) \quad (10)$$

$$(11)$$

where $\Delta x = [\Delta\delta_{g,i}, \Delta\omega_{g,i}, \Delta P_{m,i}, \Delta P_{g,i}, \Delta\delta_{es,s}, \Delta\omega_{es,s}, \Delta P_{f,s}]^T$ is the state vector, $u = P_{ref,s}$ is the control signal of the embedded storage, Δw is the load disturbance, A_d, B_d, F_d are the state space matrices.

Two control objectives are considered: firstly, to minimize the total control effort of the storage system throughout the prediction horizon, and secondly, to reduce frequency deviation.

$$\min \mu \sum_{k=1}^K \sum_{s=1}^S \|P_{ref,s}(k)\| + (1 - \mu)(f_{Col} - f_{ref})^2, \quad (12)$$

where μ is the weighting factor, K is the prediction horizon, S is the total number of the embedded storage.

The Center of Inertia (Col) frequency is used in this study to represent the network frequency,

$$\omega_{Col} = \frac{\sum_{s=1}^S H_{es,s}\omega_{es,s} + \sum_{i=1}^M H_{g,i}\omega_{g,i}}{\sum_{s=1}^S H_{es,s} + \sum_{i=1}^M H_{g,i}} \quad (13)$$

Taking into account the previously mentioned objectives, the optimal control signal of the storage is addressed while considering constraints such as the rate of change of frequency (RoCoF), frequency deviation, and operational limits of both the conventional generator and the storage, as shown below:

$$|\omega_{\text{Col}}(k)| \leq \omega_{\text{lim}} \quad (14)$$

$$\frac{d}{dt}\omega_{\text{Col}}(k) = \frac{\omega_{\text{Col}}(k) - \omega_{\text{Col}}(k-1)}{T_s} \quad (15)$$

$$\left| \frac{d}{dt}\omega_{\text{Col}}(k) \right| \leq \omega_{\text{lim}}^{\text{rate}} \quad (16)$$

$$\text{SoC}_s(k+1) = \text{SoC}_s(k) + \frac{P_{es,s}(k)T_s}{E_{b,s}} \quad (17)$$

$$\text{SoC}_{\min} \leq \text{SoC}_s(k) \leq \text{SoC}_{\max} \quad (18)$$

$$0 \leq P_{m,i}(k) \leq P_{g,i}^{\text{nom}} \quad (19)$$

$$\left| \Delta P_{\text{ref},s}(k) - \frac{1}{m_p}(\omega_{es,s} - \omega_{\text{ref}}) \right| \leq P_{es,s}^{\text{nom}}. \quad (20)$$

Constraint (14) reflects the frequency deviation limits. Constraint (16) reflects the RoCoF limits. Constraint (18) reflects the state of charging limits of the storage. Constraints (19)-(20) reflect the power limits of the synchronous generator and the storage.

1.3 Case Studies

We test the proposed control in a modified IEEE 39 bus system as shown in Fig. 1. We have installed embedded storage units at bus 4, bus 8, bus 16, and bus 20. Assuming that the total nominal power of these four embedded storage units is 10% of the total load in the system, the parameter settings for all four storage units are identical. The nominal power of each storage is 157 MW. The inertia gain is 12 s. The damping gain is 1. The power output is defined in per unit, The SoC limits of the battery are set to 0 and 1. T_s is 0.1 s and the prediction horizon length is 0.5 s. The Interior Point Optimizer (IPOPT) is utilized to solve the optimization problem.

We set the frequency deviation limit to ± 0.6 Hz and the RoCoF limit to ± 0.6 Hz/s. Assuming a sudden 900 MW load increase at bus 3 at 5 s, the Col frequency and the optimal reference of the storage at bus 4 without the optimal control, with the optimal control and $\mu = 1$, with the optimal control and $\mu = 0.5$ are depicted in Fig.2. It can be observed from the figure that the frequency nadir is 59.317 Hz without optimal control, which may lead to load shedding. Conversely, with optimal control, the frequency nadir increases to 59.4 Hz. The optimal control signal corresponding to the load disturbance is dispatched to the embedded storage. During the quasi-steady state, the frequency stabilizes at 49.4 Hz, eliminating the need for an additional active power reference. Furthermore, when we take into account the minimization of frequency deviation alongside reducing the control impact of the storage, the steady-state frequency nadir increases to 59.556 Hz, and the steady-state frequency rises to 59.597 Hz. As a result, the storage system must deliver a greater control effect.

We also consider another scenario where the frequency deviation limit is ± 0.5 Hz and the RoCoF limit is ± 0.5 Hz/s. The same load disturbance occurs, and the optimal power reference of the storage at bus 4, along with the Col frequency under optimal control and $\mu = 1$ is shown in Fig. 3. It is evident that ensuring the frequency remains within the specified limits after the load disturbance necessitates an additional control signal not only immediately after the disturbance but also during the quasi-steady state.

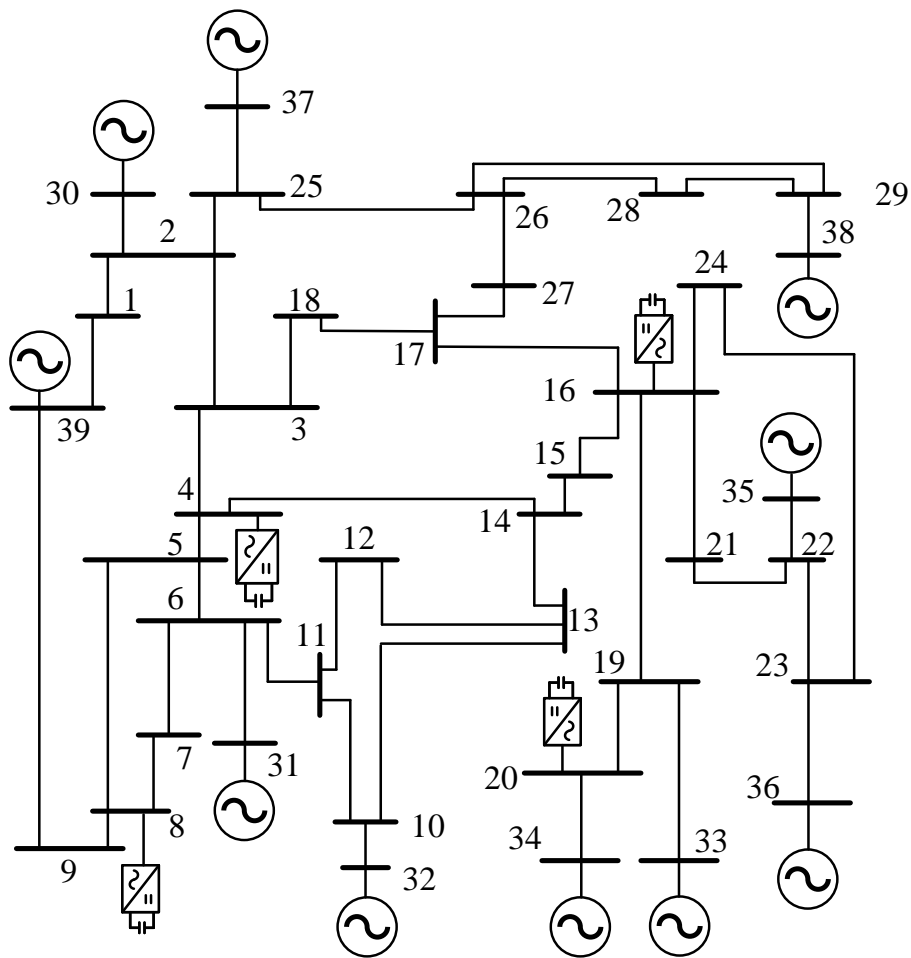


Figure 1: Modified IEEE 39 bus system

1.4 Conclusion

This study introduces an optimal control strategy for achieving rapid frequency response in VSM-controlled GFM embedded storage. We design an upper-layer control for the storage utilizing receding horizon optimization. Various scenarios are tested in case studies, and simulation outcomes confirm that without our proposed control, the frequency may exceed specified limits, potentially leading to load shedding. Conversely, the proposed control ensures the frequency remains within the designated bounds. Furthermore, our control method not only focuses on minimizing the overall control effort from the embedded storage but also addresses enhancements in frequency behavior.

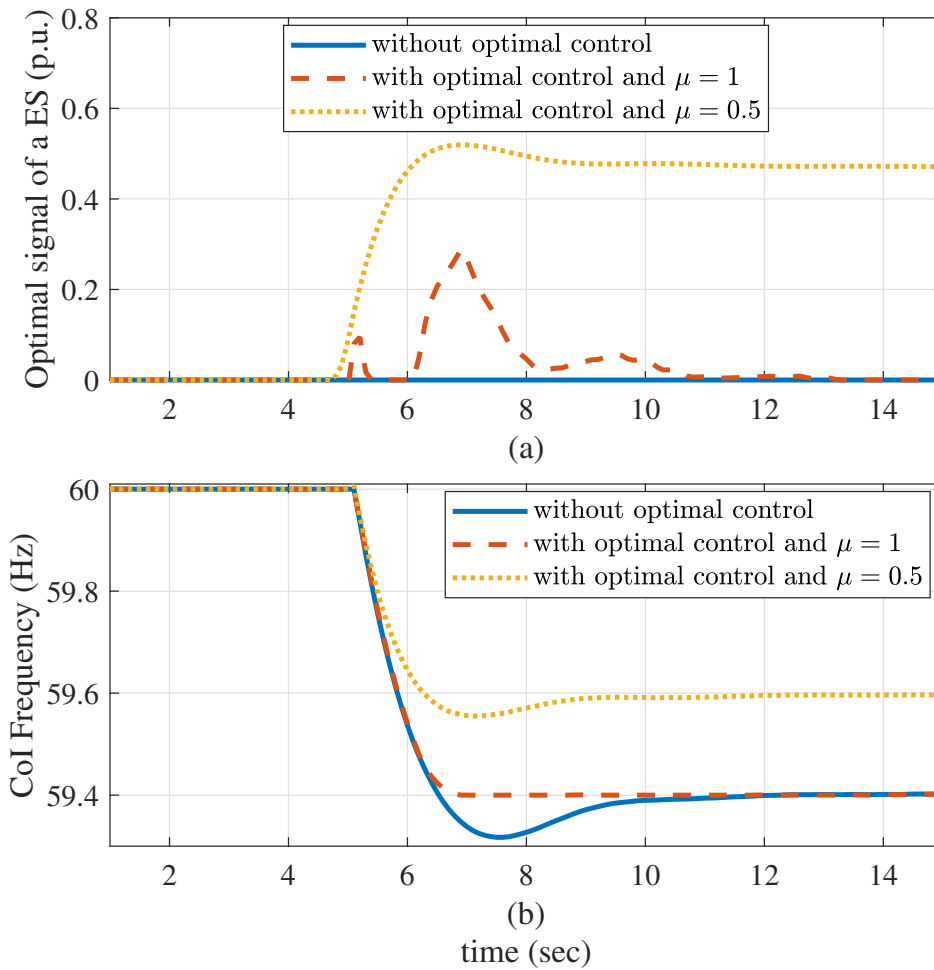


Figure 2: Simulation result under scenario 1 (a) Optimal active power reference of the storage at bus 4, (b) CoI frequency.

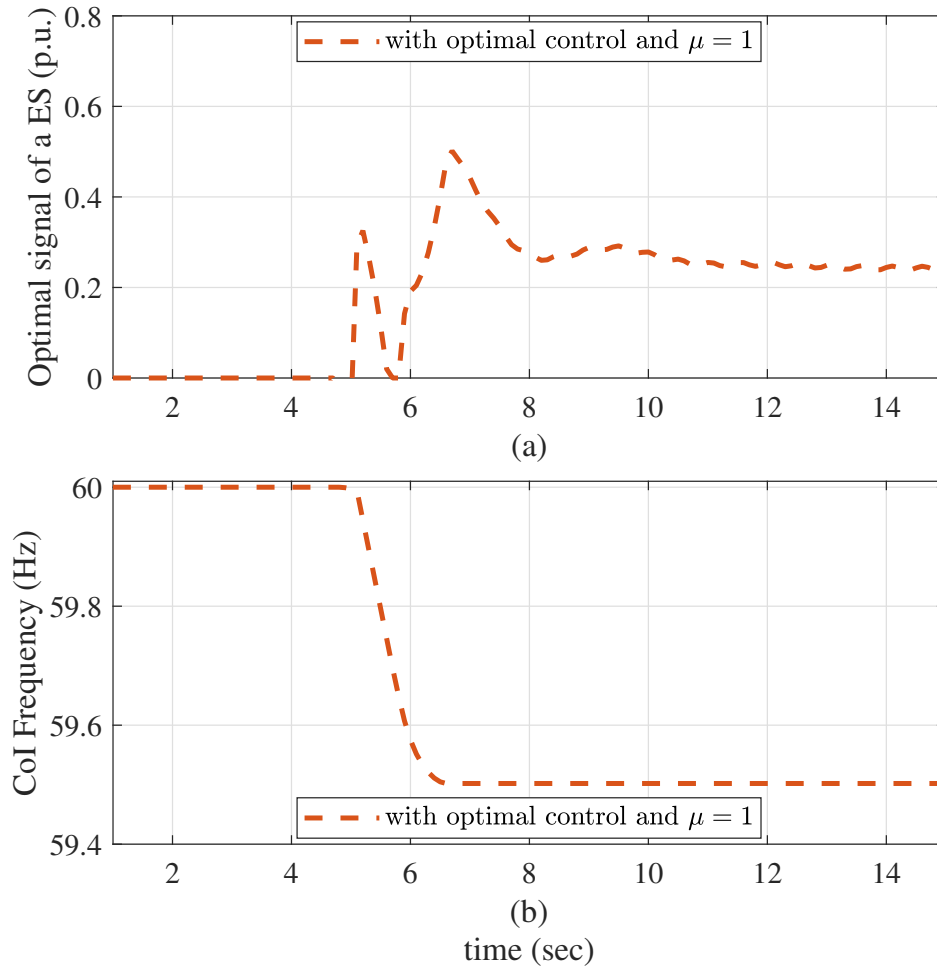


Figure 3: Simulation result under scenario 2 (a) Optimal active power reference of the storage at bus 4, (b) CoI frequency.

2.0 Optimal Scheduling of Mobile Embedded Storages with Grid-Forming Control for Black-Start

2.1 Background & Inspiration

Most commonly-used black-start generators are hydro and diesel generators. However, with the increasing penetration of inverter-based generation (IBG) - wind, photovoltaics (PV), battery energy storage systems (BESS), their capability and potential to provide black-start support are of most interest.

Typically, there are three stages included in power system restoration after a black-out: preparation and black-start allocation, transmission system energization, and load recovery. The main focus of this research is based on the first two stages that ensure fastest energization of transmission corridor which provides cranking power for non black-start (NBS) generators as well as keep the system reliable and stable.

2.2 New Problem Formulation

2.2.1 Assumptions

- Assume DC power flow
- Assume cranking power of each NBS generator is about 10% of maximum generation.
- Assume that all existing generators are NBS
- Assume that mobile energy storage (MES) are the only BS resources
- Assume each MES has a 4-hour period with 200MW capability (800MWh in total)
- Assume the distance between two adjacent buses is the same (one mile), and the move distance of MES is one unit per time step.

2.2.2 Modeling of mobile embedded storages

- Assume there are multiple embedded storages (but we can start with 2 storages as a starting point)
- Assume MES only discharges during this entire blackstart process
- MES mainly provides the cranking power to NBS generators which means the NBS should be energized ASAP. Once the NBS generators are energized, they should support the loads at their maximum capability.
- When modeling the mobility of embedded storages, there should be a binary variable w.r.t bus number, storage index, and time.
- **Need to take transportation time into account, with a constant speed for all storages.**

2.2.3 Variables of the system

i : bus number;

D_i : demand at bus i ;

$P_{l,t}$: power flow along line l at time t ;

$LS_{i,t}$: load shedding at bus i at time t ;

$P_{G,i,t}$: power generation by generator located at bus i at time t ;

$P_{mes,i,D}$: discharged power by MES located at bus i ;

$P_{mes,cap}$: discharge capacity of MES per hour;

v_{mes} : move speed of MES;

$d_{mes,i}$: distance to another MES station when MES located at bus i ;

$T_{mes,i,t}$: transportation time of MES located at bus i at time t

Binary Variables:

η : line status (0: line out of service; 1: line in-service);

$\beta_{nbs,i,t}$: NBS status (0: NBS not energized; 1: NBS is energized)

$\mu_{mes,i,t}$: status of MES located at bus i (0: MES out of service; 1: MES in-service);

$\tau_{mes,i,t}$: status of MES transportation (0: MES is fixed; 1: MES is moving)

2.2.4 Objective function

$$\min \sum_{t=1}^T \left[\sum_{i \in B} LS_{i,t} + 10 * \sum_{i \in B} P_{crank,i} * (1 - \beta_{nbs,i,t}) \right] \quad (21)$$

2.2.5 Constraints

Power balance equation:

$$\sum P_{l,t} - \sum P_{l,t} + P_{mes,i,D}^t + P_{G,i,t} + LS_{i,t} = D_i \quad (22)$$

Based on one of the assumptions, before the NBS generators get energized:

$$P_{G,i} = -P_{crank,i} = 0.1P_{G,i}^{max}$$

where P_{crank} is the cranking power needed by NBS generators to get energized. After the NBS generator is energized, it can generate power to the system within the limits,

$$P_{G,i}^{min} \leq P_{G,i,t} \leq P_{G,i}^{max}$$

The status of NBS is determined by the power flew to it, and it can operate as a generator only when it get energized.

Line capability limits:

$$\eta P_l^{min} \leq P_{l,t} \leq \eta P_l^{max} \quad (23)$$

where η is a binary variable that represents whether the line has been in-service or not.

Embedded Storage:

$$\begin{aligned} \mu_{mes,i,t} * P_{mes,D}^{min} &\leq P_{mes,i,D}^t \leq \mu_{mes,i,t} * P_{mes,D}^{max} \\ P_{mes,i,D}^t &\leq \mu_{mes,i,t} * P_{mes,cap} \\ \sum \mu_{mes,i,t} &\leq N \end{aligned} \quad (24)$$

where N is the number of available embedded storage at time t .

Since only the discharge status of MES is considered at current stage, its maximum capacity should be updated after each time step,

$$P_{mes,i,D}^t \leq P_{mes,D}^{max} - \sum_{t'=1}^{t-1} P_{mes,i,D}^{t'}, \quad t \geq 1 \quad (25)$$

The MES move speed v_{mes} , MES stations, and the distance between two stations $d_{mes,i}$ are pre-defined.

$$T_{mes,i,t} = d_{mes,i}/v_{mes} \quad (26)$$

When the MES is moving, it cannot work. Therefore,

$$\sum_t^{t+T} \mu_{mes,i,t} \leq 1 \quad (27)$$

$$\tau_{mes,i,t} = 1 - \mu_{mes,i,t}$$

2.3 Simulation Results

To validate the effectiveness of the proposed algorithms and formulations, a simulation based on 9-bus system which is shown in Figure 4 was performed.

In this system, there are 2 NBS generators, 2 MES stations and 1 MES. The distance between the two MES stations is 2 miles, and the move speed of the MES is $1/mph$. The detailed information of this system is shown in Table 1.

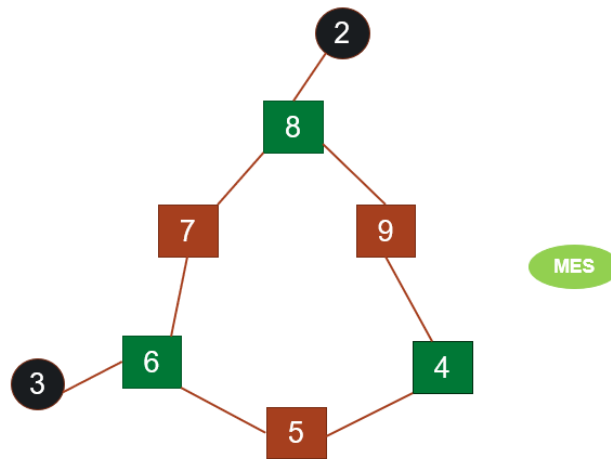


Figure 4: Overview of 9-bus system

Bus number	2	3	4	5	6	7	8	9	-
Property	NBS	NBS	MES station	Load	MES station	Load	MES station	Load	MES
MW	300	270	0	90	0	100	0	125	

Table 1: System information of 9-bus system

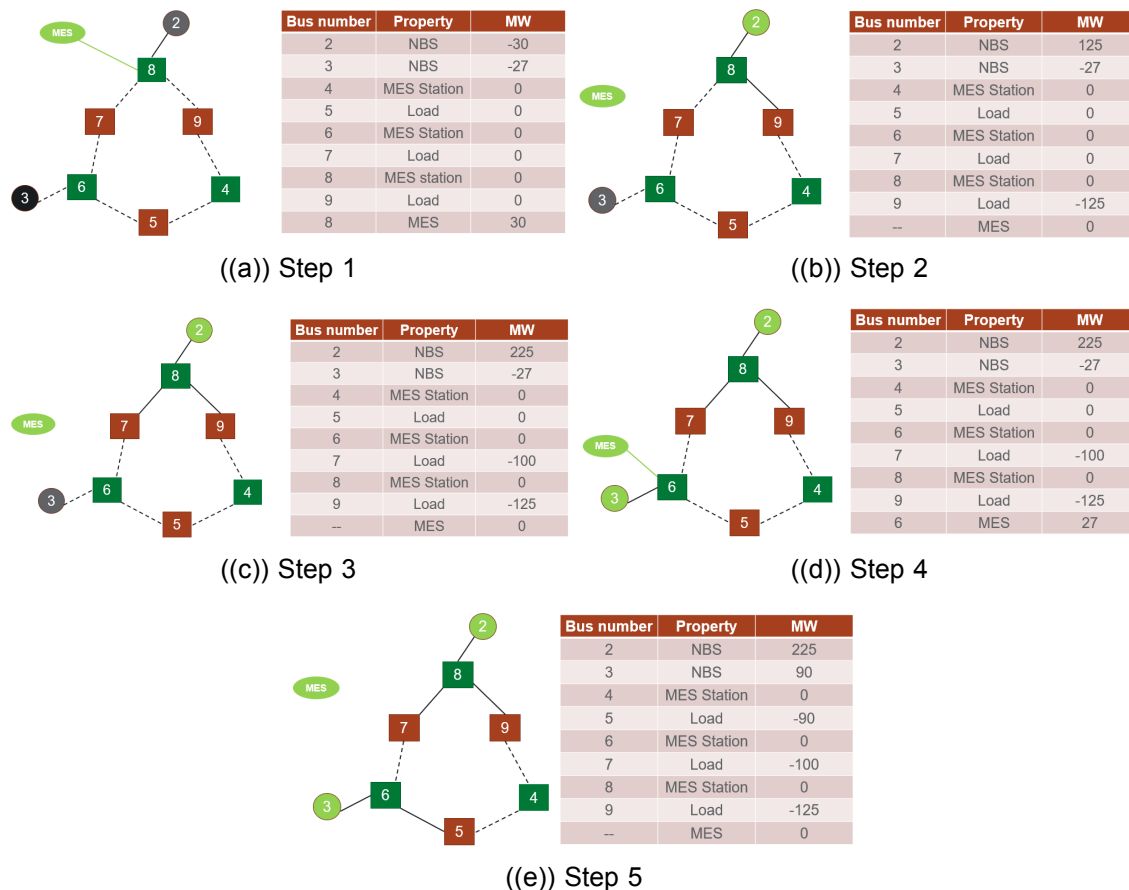


Figure 5: Recovery Process of 9-bus Power System (red rectangular with bus number: loads; green rectangular with bus number: MES stations; black circle with bus number: NBS unit; grey circle with bus number: NBS unit is energized; black lines: recovered/normal transmission lines; dashed lines: destroyed transmission lines).

During the simulation, only 1 transmission line can be recovered per time step. The simulation results are shown below, From Figure 5, it is clear that the MES first energizes NBS located at bus 2 since it needs more cranking power to be energized. Then, the MES takes 2 time steps to move to bus 6 to energize the NBS at bus 3. Meanwhile, the NBS at bus 2 begins to operate as a generator after getting the cranking power and pick up the loads in the system. After the NBS at bus 3 gets energized, it helps to recover the whole system as well.

The comparison of the optimal solutions versus an non-optimal solution is shown in Table 2.

time step	optimal solution	non-optimal solution
1	612	760
2	460	695
3	360	885
4	90	885
5	0	612

Table 2: Comparison of the optimal and non-optimal solution.

References

- [1] M. C. Chandorkar, D. M. Divan, and R. Adapa, "Control of parallel connected inverters in standalone ac supply systems," *IEEE transactions on industry applications*, vol. 29, no. 1, pp. 136–143, 1993.
- [2] J. Rocabert, A. Luna, F. Blaabjerg, and P. Rodriguez, "Control of power converters in ac microgrids," *IEEE transactions on power electronics*, vol. 27, no. 11, pp. 4734–4749, 2012.
- [3] Q.-C. Zhong and G. Weiss, "Synchronverters: Inverters that mimic synchronous generators," *IEEE transactions on industrial electronics*, vol. 58, no. 4, pp. 1259–1267, 2010.
- [4] B. K. Poolla, D. Groß, and F. Dörfler, "Placement and implementation of grid-forming and grid-following virtual inertia and fast frequency response," *IEEE Transactions on Power Systems*, vol. 34, no. 4, pp. 3035–3046, 2019.
- [5] U. Markovic, Z. Chu, P. Aristidou, and G. Hug, "Lqr-based adaptive virtual synchronous machine for power systems with high inverter penetration," *IEEE Transactions on Sustainable Energy*, vol. 10, no. 3, pp. 1501–1512, 2018.
- [6] J. Gouveia, C. Moreira, and J. P. Lopes, "Rule-based adaptive control strategy for grid-forming inverters in islanded power systems for improving frequency stability," *Electric Power Systems Research*, vol. 197, p. 107339, 2021.

Pacific Northwest National Laboratory

902 Battelle Boulevard
P.O. Box 999
Richland, WA 99352
1-888-375-PNNL (7675)

www.pnnl.gov